Earth Evolution Sciences, Vol. 11, pp. 23-30, March, 1, 2017

# The 2013 Sea of Okhotsk deep earthquake: A complex rupture within the Ringwoodite stability zone

Suguru Endo[1], Atsushi Nakao[2], Shiro Hirano[3], and Yuji Yagi[4],*

[1]*KOZO KEIKAKU ENGINEERING Inc., 4-5-3 Chuo, Nakano-ku, Tokyo 164-0011, Japan*
[2]*Graduate School of Science and Engineering, Tokyo Institute of Technology, Ookayama 2-12-1, Meguro-ku, Tokyo 152-8551, Japan*
[3]*Department of Physical Sciences, College of Science and Engineering, Ritsumeikan University, Nojihigashi 1-1-1, Kusatsu 525-8577, Japan*
[4]*Faculty of Life and Environmental Sciences, University of Tsukuba, Tennodai 1-1-1, Tsukuba 305-8572, Japan*

**Abstract**

In 2013, a large deep earthquake occurred at the sea of Okhotsk. Some researchers have indicated the complex rupture process of this earthquake. However, there is still a lack of information about the rupture process, especially obtained by a high frequency analysis. Thus, we investigated the precise source process of the 2013 Sea of Okhotsk deep earthquake by using hybrid back-projection and waveform inversion. We found that the rupture first propagated northeastward and then southeastward. Both the high-frequency radiation and slip rate increased subsequently near the hypocenter, suggesting rupture reactivation near the hypocenter. This reactivation of the rupture shows the stress concentration near the rupture initiation. On the other hand, the temperature of the slab at the hypocentral depth estimated by our thermal structure model was higher than the boundary temperature of the metastable olivine (MO) to ringwoodite phase transition. This result may indicate that the mainshock of the Okhotsk earthquake occurred within the ringwoodite stability zone and that the transformational faulting model cannot be applied to this earthquake because of the absence of a MO wedge. Considering that the focal depth of the Okhotsk earthquake is about 600 km, it is likely that the mainshock was caused by the differential contraction of the crust and mantle lithosphere due to phase transitions. If this assumption is true, the rupture reactivation revealed by our source model is not surprising.

**Keywords:** 2013 Sea of Okhotsk deep earthquake; hybrid back-projection; waveform inversion; rupture reactivation near the hypocenter; metastable olivine wedge; transformation faulting

## Introduction

The 2013 Sea of Okhotsk earthquake (Mw 8.3; depth 608.9 km) is the largest deep earthquake that has been recorded within the subducting Kurile–Kamchatka slab. Previous studies of the Okhotsk earthquake reported complex rupture processes containing some sub-events (e.g., Wei et al., 2013; Zhan et al., 2014; Meng et al., 2014). According to the slip model by Wei et al. (2013), the slip can be divided into two stages (first southward rupture and second northward rupture); the second stage fills in the gaps left from the first stage rupture. Additionally, they suggested that the slip of the first stage and the second stage include three and one sub-events, respectively. From a sub-event model, Zhan et al. (2014) also proposed four sub-events, which are mostly same as those by Wei et al. (2013). In their model, the second sub-event E2 appears to propagate back toward the epicenter. In the low frequency band (0.0625–0.25 Hz), using a back projection (BP) method, Meng et al. (2014) also indicated a backward propagation of rupture. In respect to a possible mechanism for a generation of the Okhotsk deep earthquake, all of them mentioned that the ruptures propagated within a metastable olivine (MO) wedge in the Kurile–Kamchatka slab. In other words, they suggested that the nucleation and/or propagation of some ruptures can be associated with a transformational faulting model (e.g., Green and Burnley, 1989; Kirby et al., 1996).

In this study, we investigated in detail the source process of the 2013 Sea of Okhotsk earthquake by using a high-frequency (0.5–2.0 Hz) hybrid back-projection (HBP) method (Yagi et al., 2012) and waveform inversion (Yagi and Fukahata, 2011a). We can obtain the robust distribution of the high frequency radiation by using

the HBP method. Because the high frequency radiation reflects the complex rupture process (e.g., Spudich and Frazer, 1984) and the complicated rupture processes are presented by some earlier studies, it is worthwhile to obtain the spatiotemporal distribution of the high-frequency radiation. It should be noted that although there are some source models of the Okhotsk earthquake in low-frequency bands presented by previous research, as yet, we have little information obtained from the high-frequency source image of the earthquake. Accordingly, the clear source images visualized by our methods and comparison with some previous models provide possible implications of the 2013 Okhotsk deep earthquake. In addition to the analysis of the source process, we mention the possible cause of the mainshock of the Okhotsk earthquake.

**Data and Methods of Seismic Source Analysis**

The back-projection (BP) method is commonly used to image the rupture processes of large earthquakes (Ishii et al., 2005; Meng et al., 2011; Yao et al., 2012). For deep earthquakes, application of the BP method to teleseismic body waves appears to work well, because the Green's function of a deep earthquake is similar to the Dirac delta function (e.g., Suzuki and Yagi, 2011; Fukahata et al., 2014). Anelastic attenuation in the Earth commonly neglected in the BP method would be expected to produce a small time lag in the BP results. Therefore, we applied a hybrid back-projection (HBP) method (Yagi et al., 2012) to teleseismic P waves of the 2013 Sea of Okhotsk earthquake to obtain the precise spatiotemporal distribution of high-frequency radiation generated by the earthquake. We also applied an N-th root stack (with N = 3) in the HBP analysis to enhance the signal-to-noise ratio (Rost and Thomas, 2002).

Waveform inversion has been used to estimate the slip distribution of large earthquakes (Hartzell and Heaton, 1983; Ide et al., 2011). Because of the complexity of the rupture of the 2013 Sea of Okhotsk earthquake identified in previous studies (e.g., Wei et al., 2013; Zhan et al., 2014), we applied the waveform inversion method of Yagi and Fukahata (2011a), which considers the uncertainty of Green's functions. According to them, the smoothness of the slip distribution is determined on the basis of observed data and Akaike's Bayesian Information Criterion (ABIC) (Akaike, 1980). Using results of both the waveform inversion analysis and HBP analysis should provide a more detailed visualization of source processes than would be possible with either method used alone.

We selected vertical components of 149 and 47 teleseismic P waves downloaded from IRIS-DMC for the HBP analysis and inversion analysis, respectively (Fig. 1a, 1c). We manually picked P-wave first arrival times from raw waveform data and then shifted the observed waveforms (Fig. 1b, 1d). We then deconvolved the instrument responses from the raw waveform data and obtained velocity waveforms. For the HBP analysis, we applied a 0.5–2.0 Hz band-pass filter because the lateral resolution of the relatively low-frequency waveforms was insufficient for source imaging (Yao et al., 2012). For inversion analysis, we applied a 0.001–0.29 Hz band-pass filter and then resampled with 1 Hz.

The hypocenter we used (54.874°N, 153.281°E, depth 608.9 km) was determined by the U.S. Geological Survey (USGS). In both the HBP and waveform inversion analyses we considered a single fault (strike 205°, dip 8°, rake –78°), slightly modified from the Global Centroid Moment Tensor solution based on the inversion analysis. For the HBP analysis, we assumed a rectangular fault plane (120 km × 80 km; Fig. 2) with a potential source grid at 2 km spacing on the fault plane. For waveform inversion analysis, we used a 144 km × 88 km fault plane with a potential source grid at 8 km spacing on the fault plane. We calculated theoretical Green's functions for teleseismic body waves by using the program of Kikuchi and Kanamori (1991) with a sampling rate of 20 Hz. The maximum rupture front velocity we used for waveform

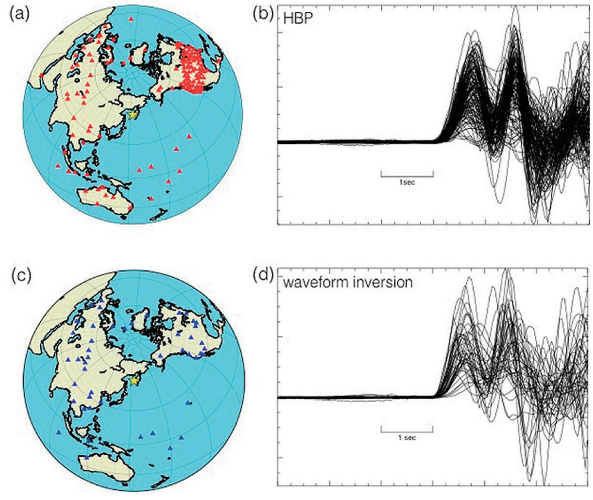


Fig. 1. Distribution of seismic stations and superposition of P waveforms. Seismic stations used for (a) hybrid back-projection (HBP) analysis and (c) waveform inversion analyses. Unfiltered vertical component P waves of the mainshock (downloaded from Data Management Center, Incorporated Research Institution for Seismology) for (b) HBP analysis at 149 stations and (d) waveform inversion analysis at 47 stations. In (b) and (d), first arrivals were picked as the first P-phase arrivals and were normalized to the maximum absolute amplitude of all waveforms. Polarity reversals were performed.

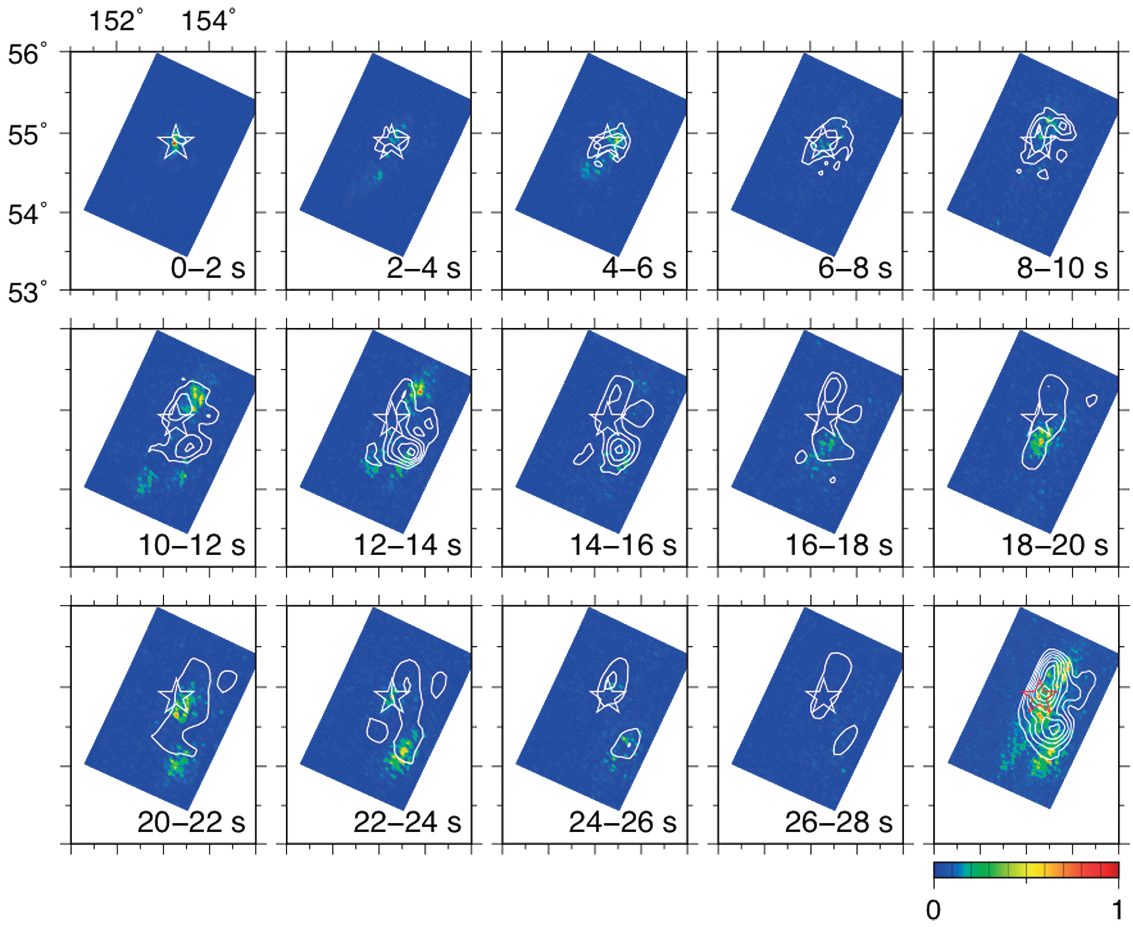


Fig. 2. Snapshots at 2-s intervals of the spatiotemporal distribution of high-frequency radiation obtained by HBP (color scale indicates normalized amplitude) with slip-rate obtained by waveform inversion (white contours, 0.22 m/s interval). Bottom right panel shows the distribution of high-frequency radiation normalized to its maximum value in the model domain with slip distribution (white contours at 1-m intervals) estimated by waveform inversion. Star indicates epicenter of mainshock.

inversion is 4.5 km/s based on the results of our HBP analysis.

**Results of Seismic Source Analysis**

Snapshots of high-frequency source radiation at 2-s intervals after rupture obtained by HBP and slip rate estimated by waveform inversion (Fig. 2) show strong initial high-frequency radiation near the hypocenter (first sub-event, SE1). From about 2 s to 12 s, high-frequency radiation propagated northeastward, with strong high-frequency radiation extending about 50 km northeast from the initial rupture point (2nd sub-event; SE2). From 12 s to 14 s, an area of high-frequency radiation developed about 60 km south-southeast of the hypocenter, and then migrated toward the hypocenter from 14 s to 20 s. From about 20 s to 24 s, high-frequency radiation occurred again near the initial rupture point (3rd sub-event; SE3). From 22 s to 26 s, high-frequency radiation also developed about 100 km south-southeast of the hypocenter (4th sub-event; SE4) and then dissipated after about 26 s. The HBP image represents abrupt changes of slip velocity (Fukahata et al., 2014), so we can interpret the strong high-frequency radiation as the drastic termination of rupture. Therefore, the sub-event SE2 and SE4 indicate the rupture termination and these events restrict the fault region. For the rupture termination, the interpretation of sub-event SE4 is consistent with the E4 in Zhan et al. (2014). The rupture duration is less than 30 s. This is in agreement with the result by Wei et al. (2013).

The slip-rate distribution (white contours in Fig. 2) shows that the rupture first propagated to the northeast and then to the southeast. Ye et al. (2013) also obtained these north and south slip. As shown in Fig. 1, the rupture area estimated by the inversion is mostly consistent with that by the HBP. We identified a re-rupture event that occurred south of the hypocenter from 20 to 22 s, which

corresponded to high-frequency radiation obtained by HBP. The HBP results indicate that the ruptures to the northeast and south-southeast of the hypocenter propagated at about 4 km/s. This rupture velocity is faster than 70% of shear-wave velocity and agrees well with rupture velocities estimated previously (Ye et al., 2013; Wei et al., 2013; Zhan et al., 2014). Considering the focal depth of about 600 km, the rupture velocities we estimated are consistent with the suggestion by Suzuki and Yagi (2011) that, at depths of 530 to 610 km, rupture velocities can be faster than 60% of the shear-wave velocity.

## Discussion

### *Complex Rupture Process*

#### *Comparison with another Source Model*

From our HBP result (Fig. 2), we can see 4 sub-events (SE1–SE4, relatively strong high-frequency radiation area): (1) at the hypocenter (0–2 s), (2) about 50 km northeastward from the hypocenter, (3) near the hypocenter (20–22 s), (4) about 100 km south-southeast of the hypocenter (22–24 s). Previous studies also identified four sub-events (E1–E4) by using an inversion method (Figure 4 in Wei et al., 2013; Fig 3 in Zhan et al., 2014). It seems that the sub-events (E1–E4) estimated by Wei et al. (2013) correspond respectively with those by Zhan et al. (2014). On the other hand, not all the sub-events (SE1–SE4) estimated by our analysis correspond with their sub-events (E1–E4). Compared to their sub-events model, we can regard SE3 near the hypocenter and SE4 in our model as E3 and E4 in the previous model, respectively. However, the SE2 appears to correspond to the E1 in the previous model. Moreover, the SE1 (strong high-frequency radiation at 0–2 s) was not detected in previous studies. On the other hand, the remarkable sub-event corresponding to E2 in the previous model is not seen in our high-frequency analysis. It must be noted that the E2 in the previous model can be explained by the slip at 14–16 s (white contours of Fig. 2 in our inversion result). It is likely that the discrepancy in the sub-events location of our model and previous models results from the discrepancy in the frequency bands used in the analyses. Our HBP analysis was conducted in higher frequency bands (0.5–2.0 Hz) compared to those of in the previous analysis (e.g., 1 Hz inversion model in Wei et al., 2013). Because high frequency waves are radiated from the rupture initiation or cessation area, the high-frequency radiation of the HBP result may be detected on the edges of the low-frequency radiation area (e.g., Nakahara, 2008).

Meng et al. (2014) or Zhan et al. (2014) also indicated the backward propagation of rupture, i.e., the southeast rupture returning toward the hypocenter in low frequency analysis. The clear backward propagation is only confirmed in 0.0625–0.25 Hz (Meng et al., 2014), while we can also detect the backward propagation in high frequency band (0.5–2.0 Hz) by using the HBP, that is, a weak high-frequency radiation at 14–20 s migrating toward the hypocenter in Fig. 2.

#### *Rupture Reactivation near the Hypocenter*

The slip model in Wei et al. (2013) shows that E3 is located at the slip gap between E1 and E2, indicating a stress concentration at the slip gap area. Of course, this interpretation can be considered reasonable, however from our source model we propose that the sub-event SE3 (same with E3 in their study) is characterized by rupture reactivation.

Recent advances in methods of earthquake analysis and the expansion of large-scale seismic networks have allowed visualization of complex earthquake source processes. Reactivation of rupture at the hypocenter (rupture initiation point) has been proposed for both the 2011 Tohoku earthquake (Ide et al., 2011) and the 2014 Iquique earthquake (Meng et al., 2015). Nielsen and Madariaga (2003) suggested that slip reactivation near the hypocenter is caused by the stress concentration near the rupture initiation point in response to growing pulses. The growing pulses (i.e., the currently slipping region) are limited behind the rupture front and their length grows proportional to the current fault length, while rupture extends along the fault.

Gabriel et al. (2012) used numerical simulations of dynamic rupture to confirm such rupture reactivation. For some of their simulations, crack-like rupture, as rupture reactivation, follows pulse-like rupture, so they called it pulse–crack superposition rupture. They found that the relative strength S, defined as the ratio of the difference of yield stress and initial stress to dynamic stress drop, is a key factor for such reactivation,

$$S = \frac{\sigma_y - \sigma_0}{\sigma_0 - \sigma_f}, \tag{1}$$

where $\sigma_y$ is the yield stress, $\sigma_0$ is the initial stress, and $\sigma_f$ is the dynamic frictional stress. A rupture is reactivated when the value of S lies between the values for pulse-like and crack-like ruptures. They also showed that the value of *S* is largely independent of nucleation size and it lies between 1 and 2 when rupture reactivation occurs. Hence we postulate that the value of *S* in our study region is between 1 and 2.

*Possible Cause of the 2013 Sea of Okhotsk Deep Earthquake*
*Transformational faulting model*

The transformational faulting model has been proposed to explain the occurrence of deep-focus earthquakes (e.g., Green and Burnley, 1989; Kirby et al., 1996). We consider that this model can be applied to the 2013 Sea of Okhotsk deep earthquake because from the viewpoint of those thermal parameters (km) the Kurile–Kamchatka slab is colder than the Bolivia slab in which the 1994 Bolivia deep earthquake occurred (Wei et al., 2013; Zhan et al., 2014; Meng et al., 2014). The thermal parameters of Kurile and Bolivia slab are about 6300 km and 1300 km, respectively (Syracuse et al., 2010). Here, the thermal parameter is defined as the product of vertical descent rate of slab and slab age. Thus, high thermal parameters reflect cold slabs.

For simplicity, we discuss the existence of the MO within the Kurile slab only based on the slab temperature, and mention the validity of the transformational faulting model for the Okhotsk earthquake. The slab temperature has a critical role in the phase transition. The maximum depth of the MO wedge strongly depends on the temperature of slabs (e.g., Devaux et al., 1997: Mosenfelder et al., 2001). If the MO exists at focal depth (about 600 km), the transformational faulting model can be valid for the occurrence of this event, as pointed out by some previous studies (Wei et al., 2013; Zhan et al., 2014; Meng et al., 2014). This is because, in the transformational faulting model, slip occurs when metastable olivine (MO) within the cold core of the slab transforms to ringwoodite.

For the calculation of the slab temperature, a simple thermal model of the slab, neglecting the temperature jump of the latent heat with 410-km and 660-km phase transition has been proposed (e.g., Kirby et al., 1996). However, a model considering the effect of the latent heat release is more realistic than the simple model (Devaux et al., 1997: Mosenfelder et al., 2001). In this study, we calculated the slab temperature, taking into account the effect of the latent heat.

We constructed a forced convection model by modifying previous free convection models (e.g., Tagawa et al., 2007) so that the features of Kurile–Kamchatka slab, such as convergence rate (8.0 cm/yr; cf. Syracuse et al., 2010), slab shape (Hayes et al., 2012), and slab age (105.6 Ma; Syracuse et al., 2010) are reproduced. The energy equation in our model contains thermal advection, thermal diffusion, heat of compression, latent heat at the 410 and 660 km phase boundaries, viscous dissipation, and internal heating by radiogenic isotopes. We assumed a dry slab, i.e., water effect to the phase transformation is neglected.

As the result of the numerical simulation, the temperature at the hypocentral depth (= 608.9 km) is higher than 700 °C (Fig. 3a). Under disequilibrium conditions, the phase transformation of MO to ringwoodite occurs at 600 °C to 700 °C (600 °C is the first phase boundary) and the ringwoodite is stable at temperatures higher than 700 °C (e.g., Rubie and Ross, 1994; Tetzlaff and Schmeling, 2000). Thus, we can simply estimate that the tip of MO wedge is about 550 km. Accordingly, the persistence of MO appears doubtful at the focal depth. Moreover, the depth of the MO tip deduced from our model can be considered as the lower limit because the wet slab has fewer MO (Hosoya et al., 2005; Kawakatsu and Yoshioka, 2011; Perrillat et al., 2013). Although we consider the uncertainty of the calculation of the temperatures (about±100 °C), it seems that our results cannot strongly support the application of the transformational faulting model to the Okhotsk earthquake. Our conclusion about the existence of the MO seems to be consistent with the distribution of the deep seismicity at depth of 370–600 km (Fig. 3b).

*Stress Concentration at depth of 600 km by Differential Contraction*

We consider another possibility of the origin of the Okhotsk earthquake. It is likely that the stress that led to the 2013 Sea of Okhotsk earthquake was concentrated in the source region because of a differential contraction (volume reduction) caused by phase transitions in the crust and mantle lithosphere (Liu and Zhang, 2015). As shown in Fig. 3c, it seems that hypocenter of the mainshock of the 2013 earthquake is not in the core of the slab; it is near the upper boundary of the slab, close to the boundary between the crust and mantle lithosphere. The depths of phase transition and the magnitude of volume changes with phase transition in MORB are different from those in harzburgite (Fig. 2 in their study). Liu and Zhang (2015) indicated that this discrepancy with phase changes results in the increase of down-dip compression toward 600 km depth. This stress concentration around 600 km depth indicates that the initial stress in the hypocentral region was relatively high. If we assume only small regional variations of yield stress and the dynamic frictional stress, the high initial stress implies a relatively low value of $S$ (see equation 1), which is consistent with the conditions for rupture reactivation proposed by Gabriel et al. (2012). The stress concentration can be potential for the generation the 2013 Sea of Okhotsk deep earthquake.

## 5. Conclusion

Our application of HBP and waveform inversion to the 2013 Sea of Okhotsk earthquake allowed us to visualize

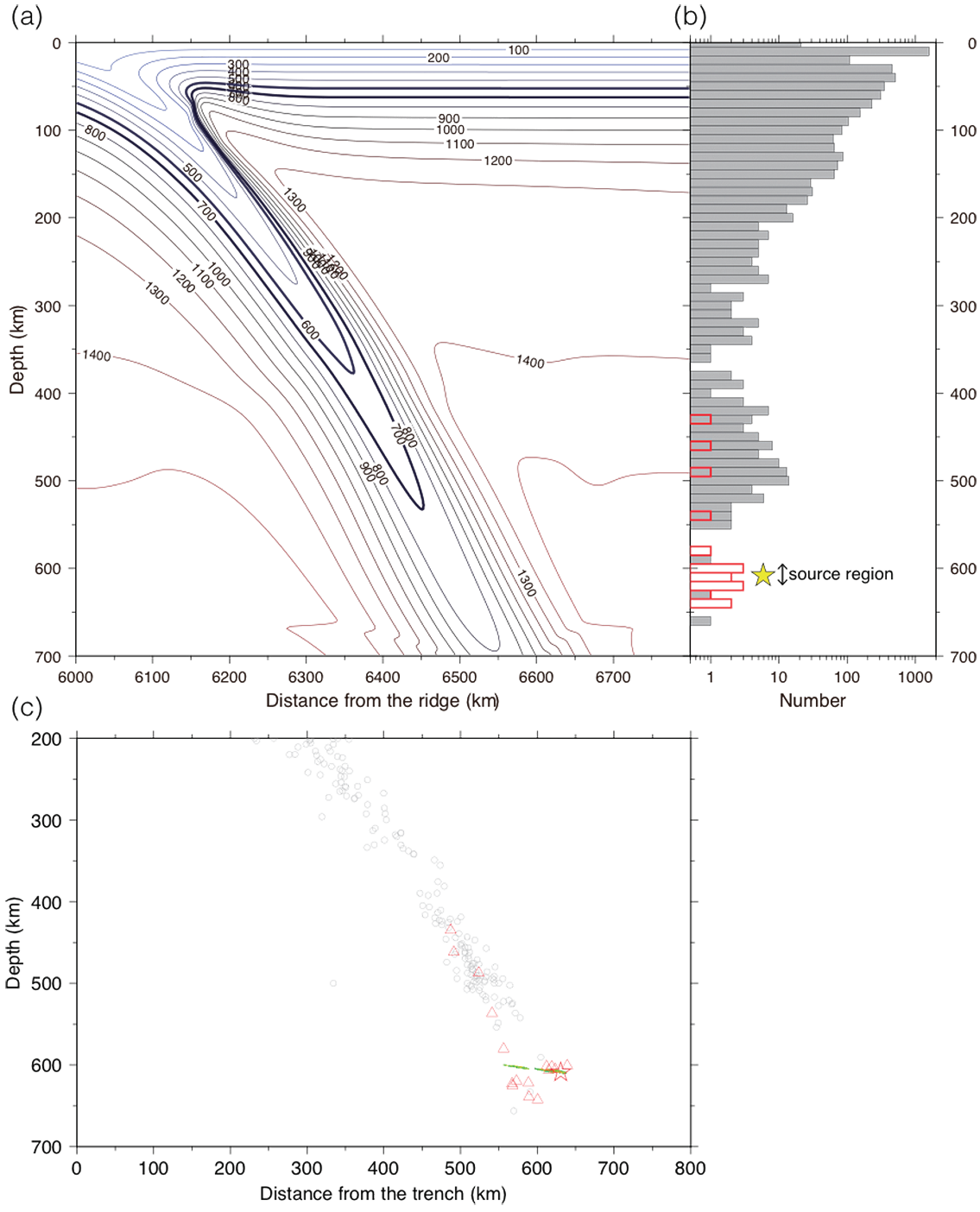


Fig. 3. (a) Cross section showing the thermal structure of the Kurile–Kamchatka slab, (b) plot of depth vs. frequency of background seismic events (Mw ≥ 4) in the Kurile–Kamchatka area and aftershocks of the 2013 Okhotsk earthquake, and (c) Cross section perpendicular to slab strike showing background seismicity and source region estimated by HBP. The horizontal axis in (a) is perpendicular to slab strike and shows distance from the mid-ocean ridge (at 0 km); the Kurile–Kamchatka trench is at 6000 km. Contours are isotherms (°C) within the slab determined by numerical simulation. For emphasis, contours at 600 and 700 °C are drawn as thick lines. All seismic events in (b) are from the Advanced National Seismic System catalog. Background seismicity (gray) is for the period from 1 January 2000 to 1 January 2015 in the region bounded by latitudes 45° to 60° and longitudes 150° and 161°. Aftershocks (Mw ≥ 4) of the 2013 earthquake up to 31 December 2013 (red) are also shown. Yellow star indicates the focal depth of the mainshock (depth 608.9 km). Gray open circles, red star, and red triangles in (c) indicate

the complex rupture process of the earthquake, including rupture reactivation near the hypocenter. The occurrence of re-rupture indicated that the *S* value in the hypocentral region was between 1 and 2. The value is relatively small, i.e., the stress concentrated near the hypocenter. We then modeled the thermal structure of Kurile–Kamchatka slab to investigate the validity of the transformational faulting model for the earthquake. Because the modeled temperature at the hypocentral depth was higher than the boundary temperature of the phase transition of MO to ringwoodite (700 °C), we concluded that the transformational faulting model could not be valid for this earthquake. This conclusion is supported by the trend of decreasing seismicity with depth; in particular, there were few seismic events in the hypocentral region. The mechanism of the 2013 Sea of Okhotsk earthquake may have been related to a differential volume contraction of crust and mantle lithosphere, which is independent of the slab temperatures. However, we need more precise estimation of the thermal structure of slab to consider a possible cause of deep earthquakes.

**Acknowledgements**

Waveform data obtained by Geoscience Australia (AU), International Federation of Digital Seismograph Networks (FDSN), Global Seismograph Network broadband stations (GSN-BROADBAND), Stations Operating STS-1 sensors (STS-1), and USArray Reference Network stations (US-REF) were supplied by the Incorporated Research Institution for Seismology (IRIS). We used hypocenters determined by the USGS. Some figures were prepared by using Generic Mapping Tools (Wessel and Smith, 1998). We thank Amato Kasahara, Ryo Okuwaki, Masanori Kurosawa, Bogdan Enescu and the Editor Katsuo Sashida for helpful comments and advices. We also thank Tomoeki Nakakuki and Hikaru Iwamori for providing us numerical programs and kind advice on the convection model we used, Numerical simulations were run on the TSUBAME 2.5 supercomputer at the Tokyo Institute of Technology. This work was supported by Grant-in-Aid for JSPS Fellows (26010035).

**References**

Akaike, H., 1980. Likelihood and the bayesian procedure. *Trabajos de Estadistica Y de Investigacion Operativa* **31**, 143–166, doi:10.1007/BF02888350.

Devaux, J. P., Schubert, G. and Anderson, C., 1997. Formation of a metastable olivine wedge in a descending slab. *Journal of Geophysical Research* **102**, 24627–24637.

Fukahata, Y., Yagi, Y. and Rivera, L., 2014. Theoretical relationship between back-projection imaging and classical linear inverse solutions. *Geophysical Journal International* **196**, 552–559, doi:10.1093/gji/ggt392.

Gabriel, A. A., Ampuero, J. P., Dalguer, L. A. and Mai, P. M., 2012. The transition of dynamic rupture styles in elastic media under velocity-weakening friction. *Journal of Geophysical Research* **117**, B09311, doi: 10.1029/2012JB009468.

Green, H. W., and Burnley, P., 1989. A new self-organizing mechanism for deep focus earthquakes. *Nature* **341**, 733–737.

Hartzell, S. and Heaton, T., 1983. Inversion of strong ground motion and teleseismic waveform data for the fault rupture history of the 1979 Imperial Valley, California, earthquake. *Bulletin of the Seismological Society of America* **73**, 1553–1583.

Hayes, G. P., Wald, D. J. and Johnson, R. L., 2012. Slab1.0: A three-dimensional model of global subduction zone geometries. *Journal of Geophysical Research* **117**, B01302, doi:10.1029/2011JB008524.

Hosoya, T., Kubo, T., Ohtani, E., Sano, A. and Funakoshi, K., 2005. Water controls the fields of metastable olivine in cold subducting slabs. *Geophysical Research Letters* **32**, L17305, doi:10.1029/2005GL023398.

Ide, S., Baltay, A. and Beroza, G. C., 2011. Shallow dynamic overshoot and energetic deep rupture in the 2011 Mw 9.0 Tohoku-Oki earthquake. *Science* **332**, 1426–1429, doi:10.1126/science.1207020.

Ishii, M., Shearer, P. M., Houston, H. and Vidale, J. E., 2005. Extent, duration and speed of the 2004 Sumatra-Andaman earthquake imaged by the Hi-Net array. *Nature* **435**, 933–6, doi:10.1038/nature03675.

Kawakatsu, H. and Yoshioka, S., 2011. Metastable olivine wedge and deep dry cold slab beneath southwest Japan. *Earth and Planetary Science Letters* **303**, 1–10.

Kikuchi, M., and Kanamori, H., 1991. Inversion of complex body waves-III. *Bulletin of the Seismological Society of America* **81**, 2335–2350.

Kirby, S., Stein, S., Okal, E. and Rubie, D., 1996. Metastable mantle phase transformations and deep earthquakes in subducting oceanic lithosphere. *Reviews of Geophysics* **34**, 261–306.

Liu, L. and Zhang, J. S., 2015. Differential contraction of subducted lithosphere layers generates deep earthquakes. *Earth and Planetary Science Letters* **421**, 98–106, doi:10.1016/j.epsl.2015.03.053.

Meng, L., Inbal, A. and Ampuero, J.P., 2011. A window into the complexity of the dynamic rupture of the 2011 Mw 9 Tohoku-Oki earthquake. *Geophysical Research Letters* **38**, 1–6, doi:10.1029/2011GL048118.

Meng, L., Ampuero, J. P. and Burgmann, R., 2014. The 2013 Okhotsk Deep-Focus Earthquake: Rupture

Beyond the Metastable Olivine Wedge and Thermally-Controlled Rise Time near the Edge of a Slab. *Geophysical Research Letters* **41**, 3779–3785, doi:10.1002/2014GL059968.

Meng, L., Huang, H., Bürgmann, R., Ampuero, J. P. and Strader, A., 2015. Dual megathrust slip behaviors of the 2014 Iquique earthquake sequence. *Earth and Planetary Science Letters* **411**, 177–187, doi:10.1016/j.epsl.2014.11.041.

Mosenfelder, J. L., Marton, F. C., Ross, C. R., Kerschhofer, L. and Rubie, D. C., 2001. Experimental constraints on the depth of olivine metastability in subducting lithosphere. *Physics of the Earth and Planetary Interiors* **127**, 165–180, doi:10.1016/S0031-9201(01)00226-6.

Nakahara, H., 2008. Seismogram Envelope Inversion for High-Frequency Seismic Energy Radiation from Moderate-to-Large Earthquakes. *Advances in Geophysics* **50**, 401–426, doi:10.1016/S0065-2687(08)00015-0.

Nielsen, S. and Madariaga, R., 2003. On the self-healing fracture mode. *Bulletin of the Seismological Society of America* **93**, 2375–2388.

Perrillat, J. P., Daniel, I., Bolfan-Casanova, N., Chollet, M., Morard, G. and Mezouar, M., 2013. Mechanism and kinetics of the α-β transition in San Carlos olivine Mg 1.8 Fe 0.2 SiO 4. *Journal of Geophysical Research* **118**, 110–119, doi:10.1002/jgrb.50061.

Rost, S. and Thomas, C., 2002. Array seismology: Methods and applications. *Reviews of Geophysics* **40**, 1008, doi:10.1029/2000RG000100.

Rubie, D. C. and Ross, C. R., 1994. Kinetics of the olivine-spinel transformation in subducting lithosphere: experimental constraints and implications for deep slab processes. *Physics of the Earth and Planetary Interiors* **86**, 223–243, doi:10.1016/0031-9201(94)05070-8.

Spudich, P. and Frazer, L. N., 1984. Variable rupture velocity amd stress drop. *Bulletin of the Seismological Society of America* **74**, 2061–2082.

Suzuki, M., and Yagi, Y., 2011. Depth dependence of rupture velocity in deep earthquakes. *Geophysical Research Letters* **38**, L05308, doi:10.1029/2011GL046807.

Syracuse, E., van Keken, P. and Abers, G., 2010. The global range of subduction zone thermal models. *Physics of the Earth and Planetary Interiors* **183**, 73–90, doi:10.1016/j.pepi.2010.02.004.

Tagawa, M., Nakakuki, T. and Tajima, F., 2007. Dynamical modeling of trench retreat driven by the slab interaction with the mantle transition zone. *Earth, Planets and Space* **59**, 65–74.

Tetzlaff, M., and Schmeling, H., 2000. The influence of olivine metastability on deep subduction of oceanic lithosphere. *Physics of the Earth and Planetary Interiors* **120**, 29–38, doi:10.1016/S0031-9201(00)00139-4.

Wei, S., Helmberger, D., Zhan, Z. and Graves, R., 2013. Rupture complexity of the Mw 8.3 Sea of Okhotsk earthquake: Rapid triggering of complementary earthquakes?. *Geophysical Research Letters* **40**, 5034–5039, doi:10.1002/grl.50977.

Wessel, P. and Smith, W. H. F., 1998. New, improved version of generic mapping tools released. Eos, *Transactions American Geophysical Union* **79**, 579–579, doi:10.1029/98EO00426.

Yagi, Y. and Fukahata, Y., 2011. Introduction of uncertainty of Green's function into waveform inversion for seismic source processes. *Geophysical Journal International* **186**, 711–720, doi:10.1111/j.1365-246X.2011.05043.x.

Yagi, Y., Nakao, A. and Kasahara, A., 2012. Smooth and rapid slip near the Japan Trench during the 2011 Tohoku-oki earthquake revealed by a hybrid back-projection method. *Earth and Planetary Science Letters* **355-356**, 94–101, doi:10.1016/j.epsl.2012.08.018.

Yao, H., Shearer, P. M. and Gerstoft, P., 2012. Subevent location and rupture imaging using iterative back-projection for the 2011 Tohoku Mw 9.0 earthquake. *Geophysical Journal International* **190**, 1152–1168, doi:10.1111/j.1365-246X.2012.05541.x.

Ye, L., Lay, T., Kanamori, H. and Koper, K. D., 2013. Energy Release of the 2013 Mw 8.3 Sea of Okhotsk Earthquake and Deep Slab Stress Heterogeneity. *Science* **341**, 1380–1384, doi:10.1126/science.1242032.

Zhan, Z., Kanamori, H., Tsai, V. C., Helmberger, D. V. and Wei, S., 2014. Rupture complexity of the 1994 Bolivia and 2013 Sea of Okhotsk deep earthquakes. *Earth and Planetary Science Letters* **385**, 89–96, doi:10.1016/j.epsl.2013.10.028.